GLOBAL GROUND-BASED ELECTRO-OPTICAL AND RADAR OBSERVATIONS OF THE 1999 LEONID SHOWER: FIRST RESULTS

P. BROWN[1], M.D. CAMPBELL[1], K.J. ELLIS[2], R.L. HAWKES[3,*], J. JONES[1], P. GURAL[4], D. BABCOCK[3,5], C. BARNBAUM[6], R.K. BARTLETT[7], M. BEDARD[8], J. BEDIENT[9], M. BEECH[10], N. BROSCH[11], S. CLIFTON[12], M. CONNORS[13], B. COOKE[12], P. GOETZ[14], J. K. GAINES[7], L. GRAMER[15], J. GRAY[1], A.R. HILDEBRAND[16], D. JEWELL[17], A. JONES[1], M. LEAKE[6], A.G. LEBLANC[3, 18], J.K. LOOPER[6], B.A. MCINTOSH[19], T. MONTAGUE[20], M. J. MORROW[9], I.S. MURRAY[3, 21], S. NIKOLOVA[1], J. ROBICHAUD[1], R. SPONDOR[22], J. TALARICO[17], C. THEIJSMEIJER[1], B. TILTON[23], M. TREU[24], C. VACHON[22], A.R. WEBSTER[1], R. WERYK[1], AND S.P. WORDEN[25]

** Physics Department, Mount Allison University, 67 York St., Sackville, NB, Canada E4L 1E6 E-mail: rhawkes@mta.ca*

[1]*University of Western Ontario, London, ON, Canada*
[2]*Communications Research Centre, Ottawa, ON, Canada*
[3]*Mount Allison University, Sackville, NB, Canada*
[4]*Science Applications International Corporation, Arlington, VA, USA*
[5] *present address: Centre for Research in Earth and Space Science, York University, Toronto, ON, Canada*
[6]*Valdosta State University, Valdosta, GA, USA*
[7]*United States Air Force, Pentagon, Washington, DC, USA*
[8]*HQ United States Air Force Directorate of Weather, Washington, DC, USA*
[9]*Meteor Group Hawaii, Hawaii, USA*
[10]*Campion College, University of Regina, Regina, SK, Canada*
[11]*Wise Observatory and Tel Aviv University, Tel Aviv, Israel*
[12]*NASA Marshall Space Flight Center, Huntsville, AB, USA*
[13]*Athabasca University, Athabasca, AB, Canada*
[14]*United States Air Force, HQ AFSPC/DORW Colorado Springs, CO, USA*
[15]*North American Meteor Network, Florida, USA*
[16]*University of Calgary, Calgary, AB, Canada*
[17]*HQ USAF Space Command, Colorado Springs, CO, USA*
[18]*present address: Saint Marys University, Halifax, NS, Canada*
[19]*London, ON, Canada*
[20]*United States Air Force, Washington, DC, USA*
[21]*present address: University of Regina, Regina, SK, Canada*
[22]*Department of National Defence, Ottawa, ON, Canada*
[23]*United States Air Force, HQ AFSPC/XPXY, Colorado Springs, CO, USA*
[24]*Space and Reconnaissance Requirements Div., United States Air Force, Washington DC, USA*
[25]*HQ United States Air Force, Pentagon, Washington, DC, USA*

Earth, Moon and Planets **82–83**: 167–190, 2000.

(Received 12 June 2000; Accepted 17 August 2000)

Abstract. A total of 18 image intensified CCD detectors were deployed at 6 locations (two in Negev Desert, Israel, and one in each of the Canary Islands, Long Key in Florida, Haleakala in Hawaii, and the Kwajalein Atoll) to provide a real-time reporting system, as well as data for subsequent detailed analysis, for the 1999 Leonid shower. Fields of view ranged from 9 to 34 degrees, with apparent limiting stellar magnitudes from about +7 to +9. In addition, a dual frequency (29.850 and 38.15 MHz) automated meteor radar with directional determination capability was located in the Canadian Arctic at Alert, Nunavut and provided continuous monitoring of the shower from a location where the radiant was constantly above the horizon. Both the radar and electro-optical systems successfully recorded the activity of the shower in real time, and typical real-time activity plots are presented. Post-event analysis has concentrated on the Israel electro-optical wide field cameras and the time interval centered around the peak of the storm. About 2700 meteors have been digitized, with 680 measured for this analysis. Of these 371 were well enough determined to permit a single-station technique to yield approximate heights. Light curves and photometric masses were computed for these 371 Leonids which form the basis of the preliminary results reported in this paper. These cameras recorded Leonid meteors with peak luminosity in the magnitude range –3 to +5, corresponding to the photometric mass range 10^{-4} to 10^{-7} kg. A regression plot of photometric mass with magnitude did not indicate any change in light curve shape over the interval studied here. The peak flux as determined by the electro-optical observations was 1.6 ± 0.1 Leonid meteors of magnitude +6.5 or brighter falling on a one square kilometer area (oriented perpendicular to the Leonid radiant) per hour. This peak flux occurred at approximately 2:07 ±: 06 UT on Nov 18 1999, corresponding to solar longitude λ_o = 235.248 (epoch 2000.0). The radar results were consistent with this maximum flux rate and time. There was not a strong change in mass distribution over the few hours around maximum, although there is some indication that the peak interval was stronger in fainter meteors. Height histograms are provided for beginning, maximum luminosity and ending heights. It was found that maximum luminosity and ending heights were completely independent of mass, consistent with a dustball model in which the meteoroids are fragmented into constituent grains prior to ablation of the grains. However, the beginning height increases sharply (9.1 km per decade of photometric mass change) with increasing mass. This is possibly indicative of a volatile component which ablates early in the atmospheric trajectory.

Keywords: Leonids 1999, meteor, meteor flux, meteor shower, meteoroids, satellite impact hazard

1. Introduction

A series of distributed ground based stations can offer a cost-effective means of monitoring meteor showers. This paper will describe a network of six electro-optical locations and one multi-frequency radar location which were used to provide near real-time data on the 1999 Leonid shower to an operations control center. The main real-time goal was to provide mass-dependent flux information to satellite operators in near real time because of concern regarding the potential Leonid hazard to satellites (Beech *et al.*, 1995, 1997; Cevolani and Foschini, 1998). A secondary goal of the global ground-based campaign was to provide information on the mass distribution, atmospheric trajectories, orbits and physical structure of the Leonid meteoroids. This report provides some preliminary results from those analyses.

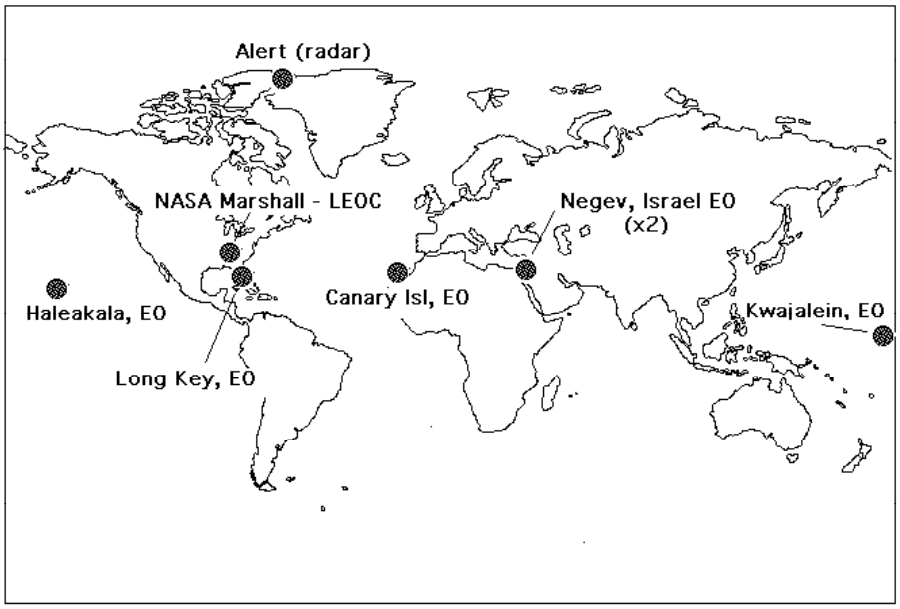

Figure 1. Map showing the location of the six electro-optical (EO) sites around the world, and the location of the dual-frequency radar in Alert, Canada, and the LEOC (LEonid Operations Control center) at NASA Marshall Space Flight Center in Huntsville, AB.

2. The network

We show in Figure 1 the observing locations used in this campaign. The central data node was located at NASA Marshall Space Flight Center in Huntsville, AL, USA. At this location, all data from the radar and electro-optical stations were processed in near real-time, with activity and predictions then forwarded to satellite operators (Treu *et al.,* 2000). The electro-optical (EO) stations were located at six different locations, all of which were somewhat near 23° north latitude, so that the radiant would be high in the sky near dawn, and were selected to provide good longitude coverage.

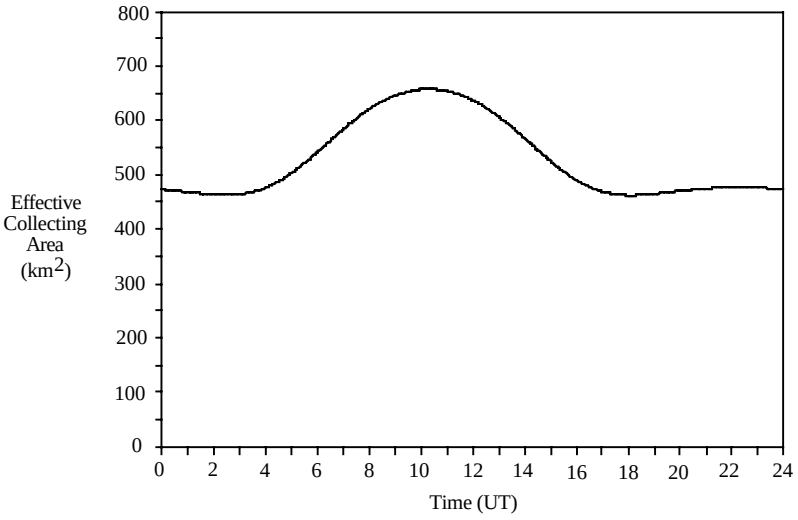

Figure 2. Effective radar collecting area for the Leonid radiant on November 18, 2000 from Alert.

The radar station was located at Alert, Nunavut, Canada (83° N, 68° W). From this location, the Leonid radiant is low in elevation but always above the horizon thus allowing for continuous observation. At this latitude, the specular reflection line for the radiant reaches almost overhead - a nearly optimum condition for radio based meteor studies. As a result, the effective echo collecting area for the radar, calculated as described in Brown and Jones (1995), varies only marginally throughout the course of a day (Figure 2). The radar system itself consists of two identical Skiymet radars that were operated in synchronism at frequencies of 29.850 and 38.150 MHz. A summary of the operational

parameters of these systems is given in Table I. To obtain directional information, identical five-antenna interferometer arrays were used at each frequency with antenna spacings of 2 λ and 2.5 λ as illustrated in Figure 3. Using this configuration, the position of the specular reflection point could be compared with each echo direction and used to discriminate against non-Leonid meteors. As the radars were equipped with fully automated meteor detection software (see report by Hocking in this volume) real-time reporting of echo rates and other quantities was possible. It should be noted that an added benefit of this system is that dual-frequency simultaneous echoes can be used to derive an echo rate correction factor that can then be used to compensate for initial trail radius effects, since the loss in echo strength will be strongly wavelength dependent.

TABLE I

Parameter	**Radar 1**	**Radar 2**
Freq. (MHz)	29.850	38.150
Pulse Width (μs)	13.3	13.3
PRF (Hz)	2144	2144
GR (dBi)	6.2	6.2
GT (dBi)	7.0	7.0
PT (kW)	3.78	6.13
# Receivers	5	5

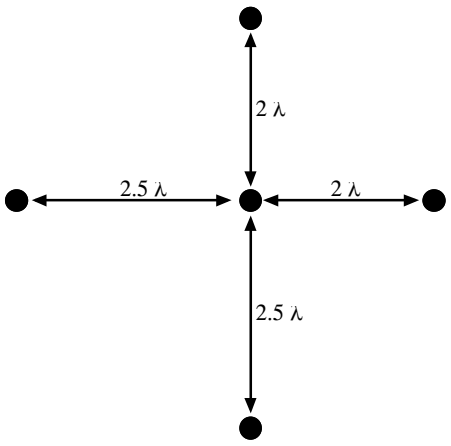

Figure 3. Interferometer spacing used in the receiving antennae.

The primary electro-optical location was in the Negev Desert in Israel. The predicted maximum of the storm would occur at about 4 am local time from this location. Two stations were set up, one at the Wise Observatory, near Mitzpe Ramon (30° 35' 45" N, 34° 45' 48" E) and the other near Revivim Kibbutz (31° 1' 45" N, 34° 42' 30" E). These were used in a triangulation mode (baseline 48.5 km) with four microchannel plate (MCP) image intensified CCD cameras at each location. Two image intensifiers at each site were generation II devices and two were generation III. The total spectral response extends from about 340 to 870 nm, although the generation III response is stronger in the red and near infrared than for the generation II systems which employ a near visual S-20 photocathode. Different focal length lenses were used at each site, resulting in different fields of view and limiting sensitivities, in order to enhance the determination of the mass distribution index. C-mount objective lenses with focal lengths from 25 to 75 mm were used, producing fields of view ranging from 35° to 9°, and a maximum limiting stellar magnitude on the most sensitive systems of nearly $+9^{m}$. The limiting meteoroid mass for the most sensitive cameras was approximately $2x10^{-8}$ kg for Leonid meteors. All CCD cameras used in the campaign were Cohu model 4910 scientific monochrome units operated at NTSC video frame rates (30 fps, with two interlaced video fields per frame). Three of the wide field cameras were equipped with MeteorScan real-time meteor detection software (Section 3).

At La Palma, in the Canary Islands (approx. 29N 16W) was located a secondary electro-optical site, with two gen II image intensified CCD cameras and two gen III image intensified CCD cameras. Each type of camera had one medium field of view (50 mm focal length lens) and one wide field (25 mm focal length) lens. Two of these cameras were used with MeteorScan automated detection software. At Long Key, FL, USA (approx. 24° 48' 48" N 80° 50' 0" W) were located two wide field gen II intensified CCD cameras, with one connected to MeteorScan automated detection. At Haleakala, HI, USA (approx. 20 N 156 W) was an electro-optical site which employed two wide angle generation III image intensified CCD cameras, with one connected to MeteorScan automated detection. At Kwajalein Atoll, Marshall Islands (approx. 9 N 167 W) was the final electo-optical site, with two generation III image intensified cameras, with one connected to MeteorScan automated detection. Unfortunately, on peak night weather conditions were poor on the

Canary Islands and at Kwajalein Atoll, and variable in Key West. Conditions were excellent at the Israel and Hawaii locations.

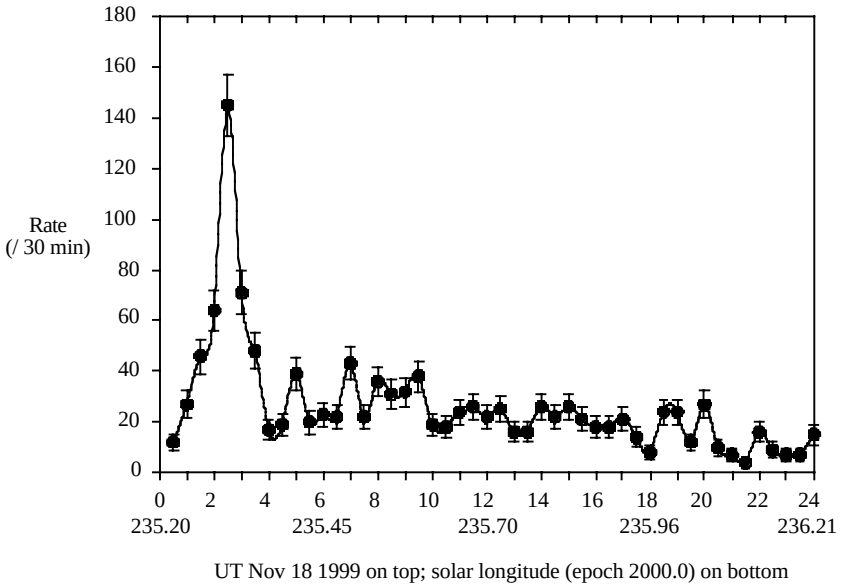

Figure 4. Automated detection results for the 38 MHz radar system for the day of Nov. 18 UT 1999. The rates are given as number of Leonids detected per 30 minute interval.

3. Real-Time Performance

Both the radar and the electro-optical systems employed real-time detection and characterization software. The output for the UT day Nov. 18 1999 for the 38 MHz radar unit is shown in Figure 4. The peak was clearly characterized by this real time data. Various real time displays could be remotely downloaded from the radar computers, including plots of radiant distribution, height distribution, flux and the echo profiles for individual events.

The electro-optical systems employed MeteorScan v2.1, developed by Pete Gural of Science Applications International Corporation (SAIC). The software runs under G3/G4 Macintosh systems, utilizing SCION LG-3 video digitizing cards. Full video frames (640x480 pixels) are digitized at 30 fps. After photometric and positional calibration, and determination of noise statistics for the CCD output, the software first performs frame subtraction to look for transient events. A noise map of

the camera is performed (and updated) so that the mean and standard deviation of pixel brightnesses are known and used to determine significant transient enhancements in pixel brightness. A Hough transform algorithm is applied to significant transient bright points in order to search for linear segments (meteors). The user has control of three settings which can be used to set the sensitivity/false alarm performance of the detection system. When a linear segment is detected, the software determines the pointing direction and angular velocity, and does a check against possible meteor showers. Statistics were reported in 15 minute intervals during the Leonid campaign, providing number of members of each shower, as well as the number of unassociated meteors. One improvement to this version of MeteorScan was the addition of a routine which integrated the light intensity of the meteor trail to obtain a measure of the meteor magnitude (after comparison with stellar data obtained in the calibration segment). Magnitude distribution information was provided by MeteorScan in real time, although these real-time magnitudes were not consistently accurate. All magnitudes reported in this paper are based on post-campaign analysis, and not on the real-time MeteorScan values.

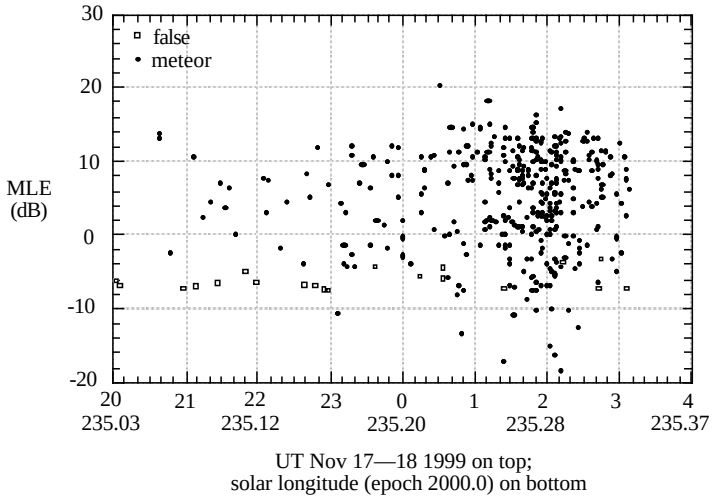

Figure 5: Plot of MeteorScan detections for one wide field camera located in Israel. The closed circles are real meteors (subsequently confirmed) while the open squares are false detections. MLE is the maximum likelihood estimator expressed in dB. It can be seen that there were very few false detections, and none of them were associated as Leonid meteors by the software.

In Figure 5 is shown the data collected from MeteorScan on peak night from one of the Israel wide field (25 mm focal length lens) cameras. The maximum likelihood estimator (MLE) in dB is plotted for each detection, with time on the x-axis. The higher the MLE the more certain the detection is a true event. After subsequent confirmation by a human observer, a different symbol was applied to meteors (circles) and false detections (open squares) in the plot. Clearly the performance of MeteorScan was outstanding, with very few false detections. None of the false detections which were recorded were incorrectly associated with the Leonids in the shower association segment of the software, so the real false detection rate of Leonids for this camera was 0%. This represented a significant improvement in MeteorScan performance over the software employed in Australia and Mongolia in the 1998 Leonid ground based campaign.

While there was some loss of MeteorScan detection efficiency during the peak of the shower, nevertheless the raw data as reported in real time accurately recorded the relative peak of the shower. In Figure 6 we show a plot of the MeteorScan output for the three Israel cameras which used real time detection, as a raw rate per 15 minute reporting interval. The maximum of the shower at approximately 2:00 to 2:10 UT Nov. 18, 1999 is evident even in these real-time data. The automated real-time reporting from both the radar and the electro-optical sites was successful.

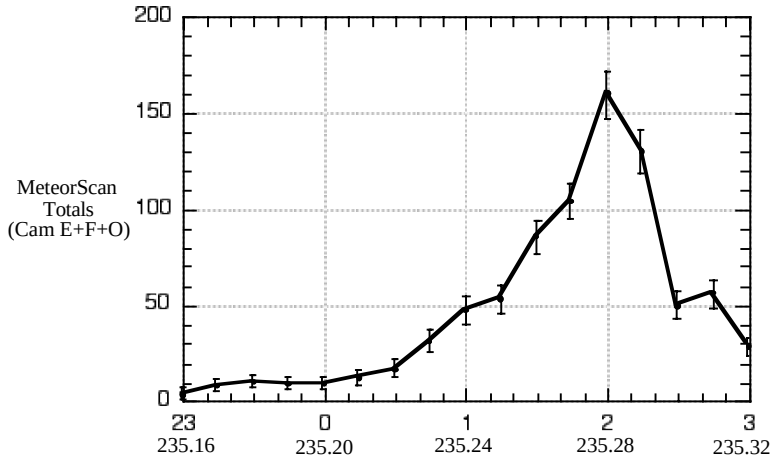

Figure 6: Real-time output of the MeteorScan automated meteor detection software on three of the wide field of view image intensified CCD cameras from Israel, reported in 15 minute intervals.

4. Post-Campaign Electro-Optical Analysis

We will now describe the post-campaign analsysis of a subset of the data collected from the electro-optical cameras. At the time of writing, the post-observation data analysis has concentrated on the cameras based in Israel, which had excellent weather during the peak of the Leonid shower. All peak-time (00–04 UT Nov 18, 1999) meteors from the Israel cameras have been digitized (~2,700 meteors, with the vast majority being Leonids). About 680 meteors have been measured, and a single station trajectory analysis (see below) performed on 371 well-measured Leonids. Magnitudes and photometric masses were determined for these 371 meteors. These data form the basis of the preliminary results presented here. It should also be mentioned that the data reported here are from the wide field of view (25 mm focal length) cameras which had a field of view of about 25° x 34° and which had an apparent limiting stellar sensitivity of about $+7.5^{m}$. The narrower field of view cameras had apparent limiting stellar sensitivity values of about $+9.0^{m}$. In this paper only the wide field results are analyzed, leaving the results of the narrow field cameras for a later paper. In the post-campaign re-analysis all meteors are redigitized (640x480x8 bit) and all meteor occurrences are human confirmed.

For positional work we employed the approach described by Hawkes *et al.* (1993). The pixel coordinates of a number of reference stars are measured, and then one applies a least squares fit between these coordinates and what an ideal (no distortion) camera would see (this is the *plate constants* approach described in detail by Wray (1967), Smart (1977), and Marsden (1982). The image measurement system provides a planar coordinate pair (x,y) for each point of interest (i.e. reference stars and meteor points). We then map (x,y) to a second planar coordinate system (ξ,η) which corresponds to what an ideal (zero distortion) system would observe. The η axis corresponds to motion along a great circle pointing in the direction of the north celestial pole, while the ξ axis points in the direction of increasing right ascension. The origin of the (ξ,η) system should be the plate center (or the reference star nearest to the plate center). Typically 15 reference stars were used in determining the positional coordinates.

Next the single station technique uses a three step process to assign shower associations. Both the direction of the meteor path and the angular velocity must be consistent with the shower. In the case of multiple shower possibilities, the best fit is assigned. Following shower association, the single-station analysis technique uses an assumed radiant and the apparent angular velocity to determine an approximate range to the meteor, and from that atmospheric trajectory information. The single station analysis technique is best suited for meteors with a relatively large number of frames, and covering a significant total angle. Under these conditions height errors may be as low as one to two km. However, in the case of meteors with only a few frames, height errors using this single station technique may be 15 km or worse. Precise dual station triangulation will be performed on meteors observed from both stations in Israel, but that data is not available for this report. Additional details on the single station analysis technique are provided by Hawkes *et al.* (1998), and it is essentially based on the pioneering work of Duffy *et al.* (1987).

For meteor photometry the method developed by Hawkes *et al.* (1993), Fleming *et al.* (1993), Campbell *et al.* (1999), and Murray *et al.* (1999) was used to determine the astronomical apparent magnitudes of these meteors. Essentially this procedure as follows. First, an area of interest (AOI) is drawn around a number of reference stars, and then a summation is obtained of the pixel intensity values over the AOI. A similar summation is obtained for background areas near the reference stars (the area just outside the star is used), and is subtracted from the reference star summation. A regression is found between the logarithm of this corrected pixel intensity summation and the astronomical magnitude, using a set of reference stars (done at the same time as the positional calibration). A similar AOI and background intensity summation is performed for the meteor points, and magnitudes obtained using the regression. Previous research on slewed stellar sources have validated this procedure (Fleming *et al.*, 1993; Campbell *et al.*, 1999).

The photometric mass is determined by integrating the meteor intensity equation (see e.g. McKinley, 1961; Ceplecha *et al.*, 1998) over the entire luminous trail of the meteor in order to obtain the following relationship for the photometric mass:

$$m_p = \frac{2}{\tau_I v^2} \int I \, dt \qquad (1)$$

We have taken the velocity term out of the integral based on the assumption there is very little deceleration over the part of the trajectory when most of the light is emitted for meteors in the size range under consideration. It is natural to expect that higher velocity meteors will be more effective in producing light. Based upon experiments at moderately low meteor velocities, it is usually assumed that the luminous efficiency factor varies linearly with velocity. If we make this assumption we obtain the following result for the photometric mass:

$$\tau_I = \tau_0 v \qquad (2)$$

$$m_p = \frac{2}{\tau_0 v^3} \int I \, dt \qquad (3)$$

For those meteors with part of the light trail outside the field of view a correction should be applied to the apparent photometric mass. We have not applied such corrections here, but we did not include photometric analyses for those meteors deemed to have significant parts of the light curve undetected. The value of the luminous efficiency parameter above is based on the work of Verniani (1965) and has the value of 1.0×10^{-10} if one places all quantities in SI units and the resulting intensity is expressed in terms of number of 0 magnitude stars (McKinley, 1961 quotes a relationship by which a 0 magnitude meteor radiates 514 W in the visual range of the spectrum). It should be stressed that the luminous efficiency factor for fast meteors, such as the Leonids, is highly uncertain, since laboratory experiments cannot be performed at these speeds. These uncertainties would influence the absolute photometric masses, but not the relative masses important for scaling mass trends.

4.1. PHOTOMETRIC MASS AS A FUNCTION OF LEONID ASTRONOMICAL MAGNITUDE

For the data from one of the cameras (E) we plot in Figure 7 the logarithm (base 10) of the photometric mass (in kg) versus the astronomical magnitude at peak luminosity. It can be seen that with this wide field intensified CCD camera the Leonid meteors had astronomical magnitudes between –3 and +5, and photometric masses between 10^{-4} kg and 10^{-7} kg. The following regression relationship is obtained between

photometric mass m, limiting astronomical magnitude at peak brightness M and the zenith angle z:

$$\textit{log}\ \text{m (kg)} = -4.98 \pm 0.02 - 0.43 \pm 0.01\ \text{M} - 0.07 \pm 0.26\ \textit{log}\ (\textit{cos}\ \text{z}) \quad (4)$$

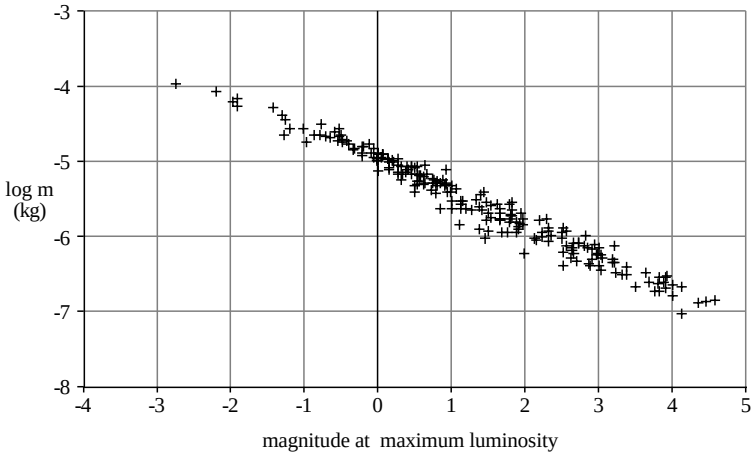

Figure 7. Plot of log photometric mass (in kg) versus meteor magnitude at peak luminosity for Leonids detected by one of the wide field intensified CCD systems.

The cos(z) dependence does not produce a statistically significant result since the meteors shown in this plot were all recorded over a very short time interval near Leonid maximum and there was insufficient variation in zenith angle. This relationship can be used to convert magnitude to photometric mass values for Leonid meteors in the magnitude range –3 to +5. If there was no change in shape of the meteor light curve with mass, one would expect a value of –0.40 for the magnitude term, which is approximated by our results. If one had a change in ablation mechanism, which resulted in changes in light curve shape, over the region investigated then the graph of log(m) versus M should not be linear. It is clear from Figure 7 that there is no indication of a dramatic change in light curve over the interval reported here. Since the relationship used to convert meteor shower population indices *r* to mass distribution indices *s* assume no change in shape of the light curve, it is important to establish the validity of this assumption.

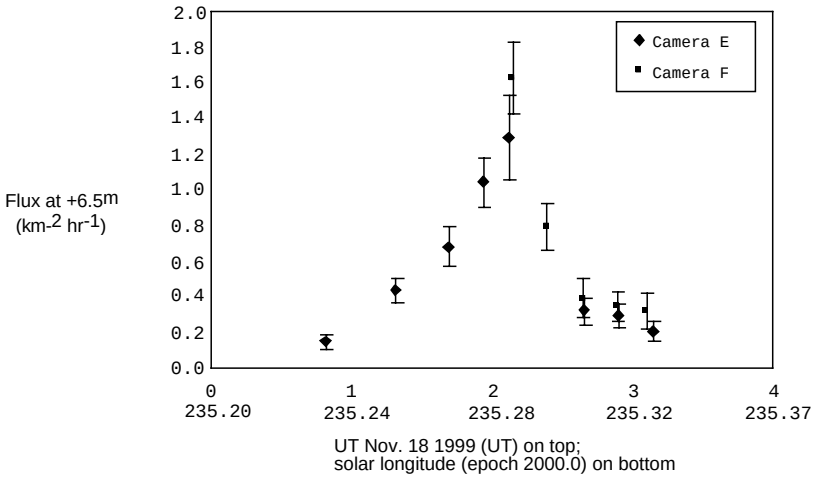

Figure 8. Meteor flux, expressed as number of Leonid meteors brighter than +6.5 magnitude which would impact on a one square kilometer surface perpendicular to the Leonid radiant plotted versus UT on Nov. 18, 1999. This is a compilation of data from two wide-field image intensified CCD cameras, with different symbols for each camera.

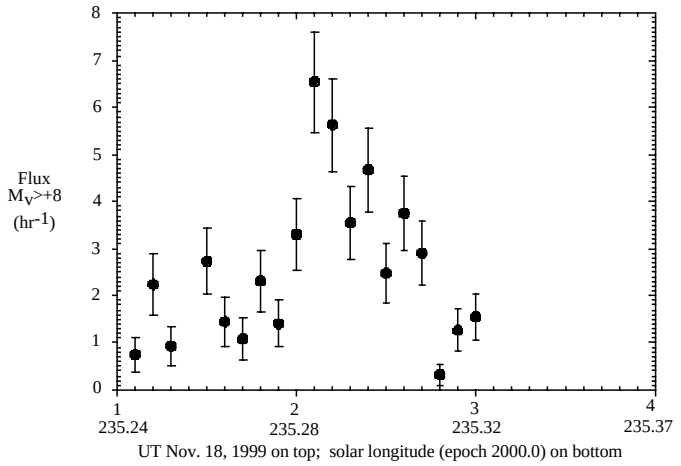

Figure 9. Leonid meteor radar flux divided into 6 minute time intervals for the 38 MHz meteor radar at Alert. The flux is to a limiting equivalent stellar magnitude of +8.

4.2. LEONID FLUX

One of the main goals of the campaign was to establish the Leonid flux in order to assess the hazard posed to satellites. While it is still early in the data analysis, we present in Figure 8 (based on the electro-optical data) a plot of the flux of Leonid meteors brighter than +6.5 astronomical magnitude versus universal time on Nov. 18, 1999. The flux is expressed in terms of number of meteors which would impact a one square kilometer surface which was oriented perpendicular to the Leonid radiant in one hour. The peak flux is 1.6 ± 0.1 Leonids brighter than $+6.5^{m}$ per square kilometer per hour, and occurs at a time of $2:07 \pm 6^{min}$ UT Nov 18 1999, which would correspond to a solar longitude value of $\lambda_o = 235.248$ (epoch 2000.0). This is consistent, within the precision of the small sample size, with the value obtained by an analysis of data from visual observers (Arlt *et al.*, 1999) which found a peak flux of 1.4 Leonid meteors brighter than $+6.5^{m}$ per square kilometer per hour, and occurs at a time of about 2:02 UT Nov 18 1999, which would correspond to a solar longitude value of λ_o=235.285 (epoch 2000.0). A detailed plot of the flux, as deduced from the 38 MHz radar, is shown in Figure 9. Here the flux is given to the radar effective limiting magnitude of +8.0. Only echoes which were within 3 degrees of the specular point from the Leonid radiant are included. We have used the radar data on November 14 (treated in the same way) as a control and subtracted these values in the same intervals to account for sporadic contamination. We have also corrected for initial trail radius effects, having computed that only 11% of all Leonid echoes are actually detected at 38 MHz, Assuming a Gaussian height distribution. This supports the idea that the maximum flux corresponded to a time of about 2:07 UT.

One interesting question is whether the mass distribution changes during the time of the intense peak. We plot in Figure 10 the photometric mass of each meteor recorded with wide field cameras E and F versus the universal time. There is no clear indication of a mass shift as the maximum is approached. Another method of looking at the data is presented in Figure 11, in which the hourly rate is reported for two different limiting photometric mass values. There is a slight hint that the central hour of most intense activity was mainly an enhancement of the fainter meteors.

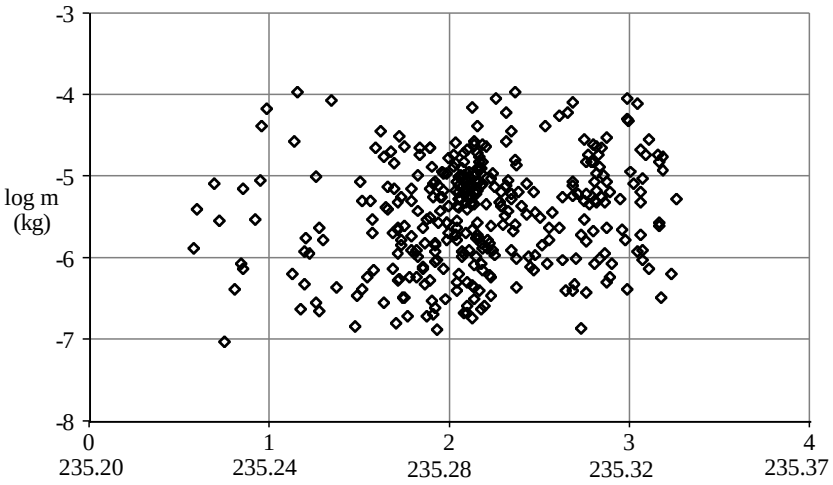

Figure 10. Plot of detections from two cameras around the time of the peak of the 1999 Leonid shower, with log photometric mass (in kg) plotted against universal time.

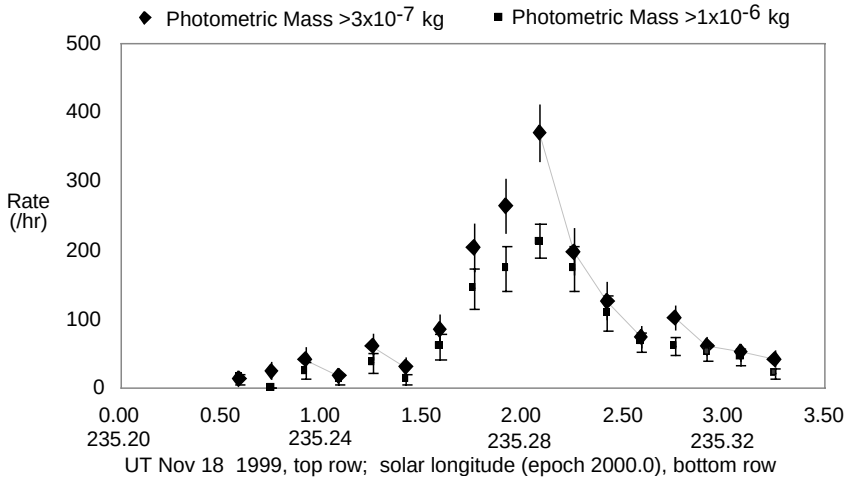

Figure 11. Meteor rate versus time (based on the electro-optical results) plotted for two limiting magnitudes (all meteors larger than 3×10^{-7} kg, and only those meteors larger than 1×10^{-6} kg). There is some hint that the peak of the shower was enhanced mainly in smaller meteors.

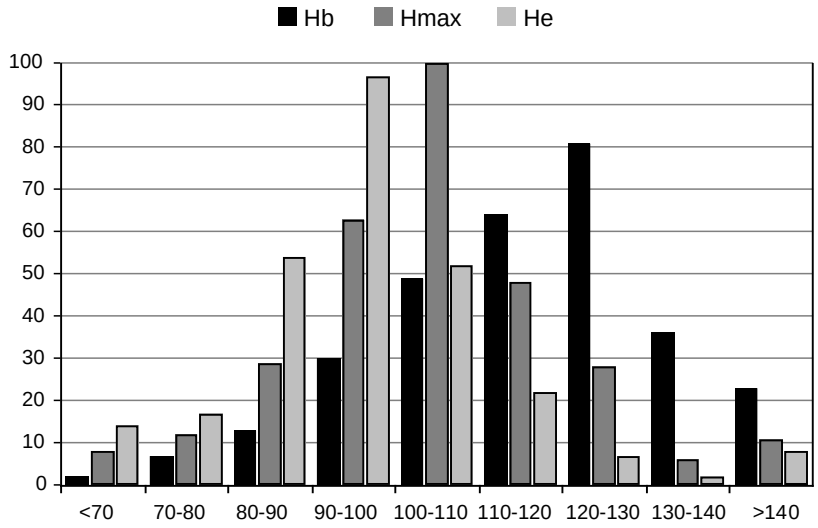

Figure 12. Histograms for beginning, maximum luminosity and ending heights for Leonid meteors. Note that uncertainties on some individual Leonids may be more than 10 km in height.

4.3. HEIGHT DISTRIBUTION

Heights of meteor atmospheric ablation profiles are one of the best indicators of the physical structure and chemical composition of meteoroids. For example, a composition rich in volatile organics would be expected to have beginning heights which are much higher than a meteoroid rich in less volatile metals. In-flight fragmentation would be expected to shorten the length of the light curves. Precision heights will await our future publication with the triangulation analysis. However, the single station procedure outlined earlier provided approximate heights. Figure 12 shows histograms of the beginning, maximum luminosity and ending heights for the meteors observed with two of the wide field of view cameras in the interval near the Leonid maximum. These results are consistent with the higher precision triangulation based heights which were measured for the 1998 Leonids (Campbell *et al.*, 2000), which indicated a mean beginning height of 114.1 km and a mean ending height of 97.1 km.

For comparison, Figure 13 shows the height distribution of Leonid echoes for all of Nov 18 at 38 MHz. Using the exact same selection

criteria, the height distribution of echoes from Nov 14 are also shown. The average height increases by almost 8 km on the night of the Leonid maximum to 98 km, with a pronounced plateau above 110 km. Indeed, two maxima are visible; one just below 100 km associated with the "sporadic" component of the selected echoes (as is also visible on November 14) and a pronounced maximum at 110 km almost certainly due to the shower. The strong drop-off above 110 km is entirely due to the initial trail radius effect, suggesting strongly that the peak in the height distribution is higher still.

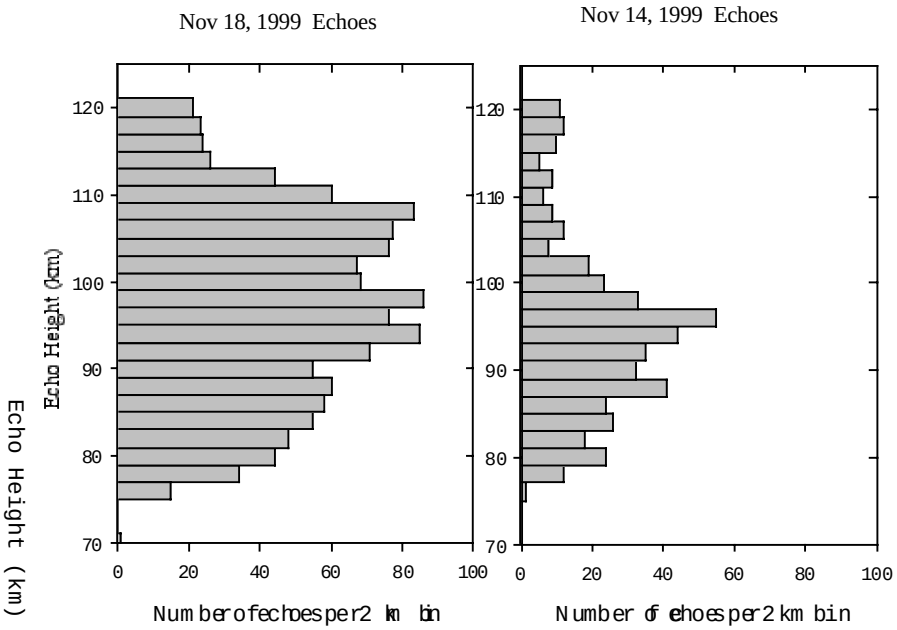

Figure 13. Radar height distribution at 38 MHz on Nov 18, 1999 (left) and on the control day Nov 14, 1999 (right). The average error in height is of order 2 km, the size of the binning used. Only echoes which were within 3 degrees of specular to the Leonid radiant are shown.

A good indicator of physical structure is how the heights vary with meteoroid mass (Hawkes and Jones, 1975). We show in Figure 14 a plot of beginning height as a function of mass, while Figure 15 shows the ending height as a function of mass. It should be kept in mind that these are low precision single-station meteor heights, so much of the scatter is simply due to the lack of precision in the technique for individual meteors.

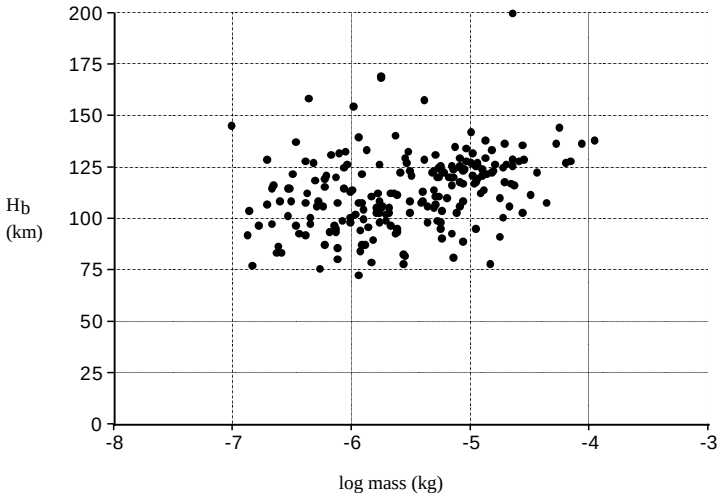

Figure 14. Plot of beginning height versus logarithm of the photometric mass of the Leonid meteoroid (in kg) based on the electro-optical observations. The best regression line shows that the beginning height increases by 9.1±1.9 km per decade mass increase.

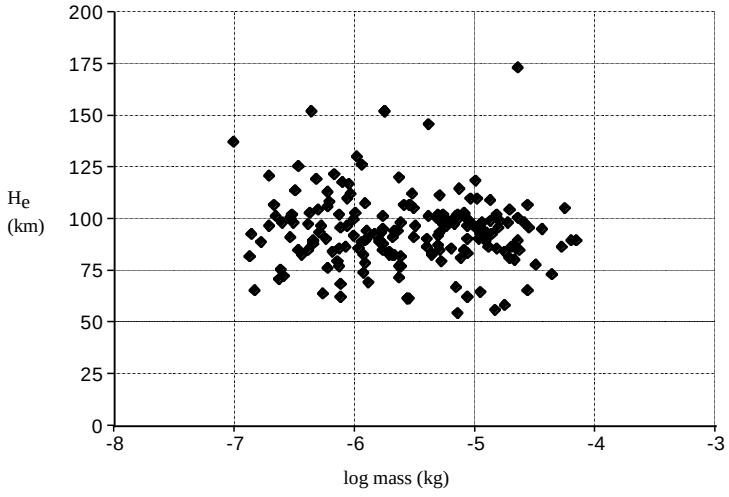

Figure 15. Plot of ending height versus logarithm of the photometric mass of the Leonid meteoroid (in kg) based on the electro-optical observations. There is no statistically significant change in ending height with meteoroid mass. A similar lack of significant change was found for the height of maximum luminosity (not shown).

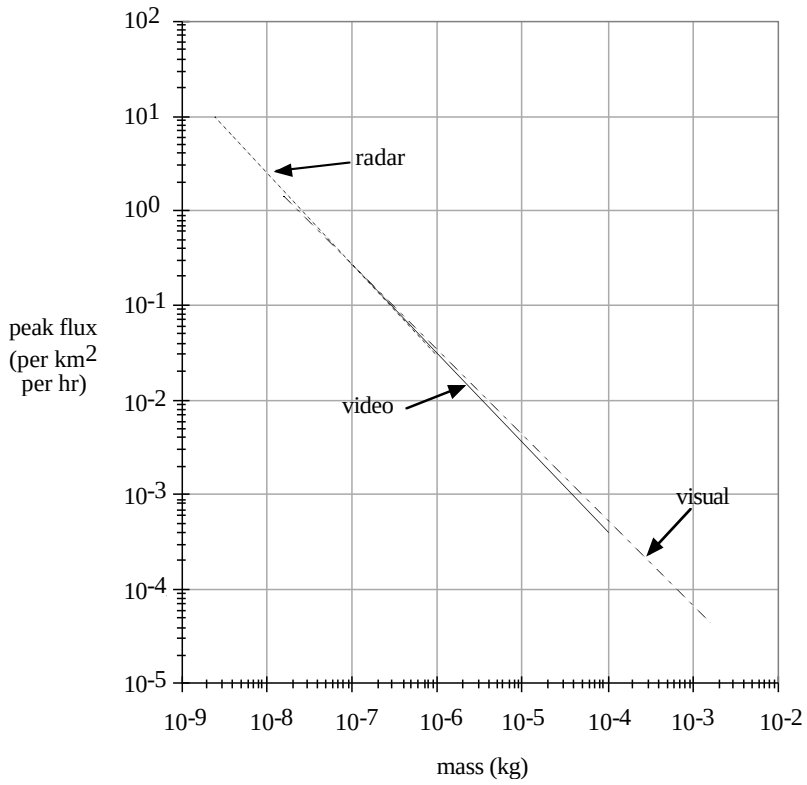

Figure 16. Measured peak flux of Leonids by radar (dotted line), video (solid line) and visual (dashed line) techniques. The flux is expressed in terms of cumulative number of meteors per square kilometer per hour which are larger than the mass value (in kg) plotted on the x-axis. Note that we have used the mass distribution indices determined by each method (radar s = 1.97; video s = 1.95; visual s = 1.90) to extend the curve over the approximate range of observations which contributed to the flux for each technique. The mass-magnitude relationship derived in this paper was used for converting magnitudes to masses in all cases.

The most interesting result is that both the maximum luminosity and ending heights showed no statistically significant dependence of heights on mass. There is some correlation of beginning height with mass (R^2 = 0.11) and the regression indicates that the mean beginning height rises by 9.1 ± 1.9 km for each increase of a factor of 10 in mass. Indeed an

extrapolation of the beginning heights to the mass regime of the bright fireballs observed by Fujiwara *et al.* (1998) would be consistent with the high heights they observe. The reason that the beginning heights should vary so strongly with mass is not obvious. It should be remembered that the difference between the limiting sensitivity of the system and the meteor increases as one goes to brighter meteors. The most exciting interpretation would be that some volatile component, which is relatively weak in light production, is ablating at great heights.

4. Discussion

Real-time flux determinations from both ground-based, globally distributed electro-optical devices and an automated dual frequency radar system were successfully demonstrated. Both techniques yielded flux values and peak times which are consistent with other observers, within the precision of the data samples. Using the measured mass distribution indices for each technique the flux as a function of mass is shown in Figure 16. For radar data the number – amplitude distribution of underdense echoes was used to determine an average value of $s = 1.97 \pm 0.02$. Visual data are from Arlt (1999) where $s = 1.90 \pm 0.05$ and TV data are from this work, where the average value for the mass index was found to be $s = 1.95 \pm 0.05$. These mass distribution indices were used to extend the measured flux over the main mass range of the observations for each of the three techniques. The mass-magnitude relationship derived earlier in this paper was used to convert observed magnitudes to masses in all cases. This suggests that the flux curve was constant over a large mass range and that no obvious turnover in the mass distribution at smaller sizes occurred before $m \sim 2 \times 10^{-9}$ kg. The three methods are in excellent agreement regarding the actual flux value.

We have provided a relationship between astronomical magnitude and photometric mass for faint Leonids. There is no indication of a dramatic change in light curve shape (which would affect this mass-magnitude regression) over the interval –3 to +5 astronomical magnitude. There is some hint that the shower was richer in faint meteors near the time of the most intense shower activity, although more data is needed to establish this conclusively.

The heights reported here indicate that the majority of the 1999 Leonids (in the size range studied here) started between 100 and 130 km

in height, had maximum luminosity points in the interval from 90 to 120 km and ended in the interval 80 to 110 km. It is interesting that there was no statistically significant dependence of ending or maximum luminosity heights on mass. This would be consistent with a physical structure (see Hawkes and Jones, 1975; also Beech, 1984) in which the meteoroid is almost completely fragmented into fundamental grains prior to the main grain ablation region of the atmosphere. However, the beginning heights did increase significantly with increasing mass. One interpretation is that a volatile component, as proposed by Elford *et al.* (1997) and Steel (1998), is ablating high in the atmosphere but producing relatively little light. For larger meteoroids the light is enough to be seen above the limiting sensitivity. The evidence for differential chemical ablation in Leonid meteors (Borovicka, 1999; von Zahn *et al.*, 1999) may be supported by this beginning height dependence on mass. Betlem *et al.* (1999) has provided precise trajectories of larger Leonids, including some very high ones, which are possibly indicative of early trail ablation of a volatile component.

One interesting question is how the height-mass dependence observed here compares with studies of sporadic meteors and those from other showers. Hawkes *et al.* (1984) and Sarma and Jones (1985) provide regression results for how heights depend on mass, velocity and other factors. They find that the beginning height does increase with increasing mass, while there is no statistically significant dependence of the height of maximum luminosity. The ending height has a slight dependence on mass, becoming lower for larger meteoroids.

Acknowledgements

The “Leonid 99” campaign reported here was funded by the US Air Force, NASA, the National Reconnaissance Office, the Canadian Space Agency, the European Space Agency, the Canadian Department of National Defence, the Defence Research Establishment Ottawa, as well as through research grants to J. Jones and R.L. Hawkes by NSERC (Natural Sciences and Engineering Research Council of Canada). The Wise Observatory and the University of Tel Aviv provided support for the campaign in Israel, the Isaac Newton Group of telescopes provided support for the campaign on La Palma. Additional support for the electro-optical sites in Maui were kindly provided by the 1st Space Surveillance Squadron, Air Force Space Command while those at the

Kwajalein Missile Range were made available through Army Space and Missile Command. *Editorial handling:* Peter Jenniskens.

References

Arlt, R.: 1999, *WGN: Journal of the IMO* **27**, 286–295.
Beech, M.: 1984, *MNRAS* **211**, 617–620.
Beech, M., Brown, P., and Jones, J.: 1995, *Q. J. R. astr. Soc*. **36**, 127—152.
Beech, M., Brown, P., Jones, J., and Webster, A.R.: 1997, *Adv. Space Res*. **20**, 1509–1512.
Betlem, H., Jenniskens, P., van Leven, J., ter Kuile, C., Johannink, C., Zhao, H., Lei, C., Li, G., Zhu, J., Evans, S., and Spurny, P.: 1999, *Meteoritics Planet. Sci*., **34**, 979–986.
Brown, P. and Jones, J.: 1995, *Earth, Moon and Planets* **68**, 223–245.
Borovicka, J., Stork, R., and Bocek, J.: 1999, *Meteoritics Planet. Sci*. **34**, 987–994.
Campbell, M.D.: 1998, *Light Curves of Faint Meteors: Implications for Physical Structure* (B.Sc. Honours Thesis, Mount Allison University, Sackville, NB, Canada.
Campbell, M.D., Hawkes, R.L., and Babcock, D.D.: 1999, in V. Porubcan and W.J. Baggaley (eds.), *Meteoroids* 1998, Astron. Institute, Slovak Academy of Sciences, Bratislava, p. 363–366.
Campbell, M.D., Brown, P.G., LeBlanc, A.G., Hawkes, R.L., Jones, J., Worden, S.P., and Correll, R.R.: 2000, *Meteoritics Planet. Sci.*, submitted.
Cevolani, G. and Foschini, L.: 1998, *Planet. Space Sci*. **46**, 1597–1604.
Duffy, A.G., Hawkes, R.L., and Jones, J.: 1987, *MNRAS* **228**, 55–75.
Elford, W., Steel, D., and Taylor, A.: 1997, *Advances in Space Research*, **20**, 1501–1504.
Fleming, D.E.B., Hawkes, R.L., and Jones, J.: 1993, in J. Stohl and I.P. Williams (eds.), *Meteoroids and Their Parent Bodies*, 261–264.
Fujiwara, V., Ueda, M., Shiba, Y., Sugimoto, M., Kinoshita, M., Shimoda, C., and Nakamura, T.: 1998,. *Geophys. Res. Lett*. **25**, 285–288.
Hawkes, R.L. and Jones, J.: 1975, *MNRAS* **173**, 339–356.
Hawkes, R.L. and Jones, J.: 1984, *Bull. Astr. Inst. Czechosl.* **35**, 46–64.
Hawkes, R.L., Mason, K.I., Fleming, D.E.B., and Stultz, C.T.:1993, in D. Ocenas and D., Zimnikoval (eds)., *International Meteor Conference 1992*, International Meteor Organization, Antwerp, 28–43.
Hawkes, R.L., Babcock, D.D., and Campbell, M.D.: 1998, *Analysis Procedures and Final Electro-Optical Results*, 31 July 1998 CRESTech Contract Report, 58 pgs.
Marsden, B.G.: 1982, *Sky & Telescope* **64**, 284.
McKinley, D.W.R.: 1961, *Meteor Science and Engineering* (New York: McGraw-Hill).
Murray, I.S., Hawkes, R.L., and Jenniskens, P.: 1999, *Meteoritics Planet. Sci*., **34**, 949–958.
Sarma, T. and Jones, J.: 1985, *Bull. Astr. Inst. Czechosl.* **36**, 9–24.
Steel, D.:1998, *Astron. Geophys* **39**, 24–26.

Treu, M., Worden, S.P., Bedard, M.G., and Bartlett, R.K.: 2000, *Earth, Moon and Planets* **82–83**, 27–38.
Verniani, F.: 1965, *Smithson. Contr. Astrophys.* **9**, 141–172.
von Zahn, U., Gerding, M., Hoffner, J., McNeil, W.J., and Murad, E.: 1999, *Meteoritics Planet. Sci.*, **34**, 1017–1027.
Wray, J.D.: 1967, *The Computation of Orbits of Doubly Photographed Meteors* (Univ. New Mexico Press, Albuquerque, U.S.A.).